Pinning analyses of a $BaHfO_3$-containing $GdBa_2Cu_3O_{7-\delta}$ thin film grown by chemical solution deposition

Pinning analyses of a $BaHfO_3$-containing $GdBa_2Cu_3O_{7-\delta}$ thin film grown by chemical solution deposition

Kazumasa Iida[1], Pablo Cayado[2], Hannes Rijckaert[3], Manuela Erbe[2], Jens Hänisch[2], Tatsunori Okada[4], Isabel Van Driessche[3], Satoshi Awaji[4] and Bernhard Holzapfel[2]

[1] Department of Materials Physics, Nagoya University, Furo-cho, Chikusa-ku, Nagoya 464-8603, Japan
[2] Institute for Technical Physics, Karlsruhe Institute of Technology, Hermann-von-Helmholtz-Platz 1, 76344 Eggenstein-Leopoldshafen, Germany
[3] SCRiPTS, Department of Chemistry, Ghent University, Krijgslaan 281-S3, 9000 Ghent, Belgium
[4] High Field Laboratory for Superconducting Materials, Institute for Materials Research, Tohoku University, Katahira 2-1-1, Aoba-ku, Sendai 980-8577, Japan

E-mail: iida@mp.pse.nagoya-u.ac.jp and pablo.cayado@kit.edu

Abstract

The electric transport properties of a $GdBa_2Cu_3O_{7-\delta}$ thin film containing 12 mol% nano-sized $BaHfO_3$ (BHO) particles grown by chemical solution deposition were investigated in a wide range of temperatures ($4.2 \leq T \leq 77$ K) and magnetic fields up to $\mu_0 H = 19$ T. The exponent n of the electric field–current density characteristics ($E \propto J^n$) depends on critical current density J_c as $(n\text{–}1) \propto J_c^{\alpha}$ ($\alpha \sim 0.45$) irrespective of measurement temperature for $H \parallel c$. On the other hand, this relation does not hold for $H \parallel ab$. The angular dependence of J_c is almost similar to that of n except for the angle close to the ab-plane. A dip of n around this angle regime was observed below 77 K, whereas J_c exhibited a maximum. At $T \leq 50$ K a tiny peak in the dip was observed that increases with decreasing temperatures. These results suggest that the pinning mechanism changes with temperature for $H \parallel ab$.

Keywords: chemical solution deposition, GdBCO thin film, electrical transport properties, BHO nano-particles

1. Introduction

$RE Ba_2Cu_3O_{7-\delta}$ (*RE*: rare earth elements, REBCO) compounds have been considered as technologically important superconductors thanks to their high critical temperature T_c as well as high critical current performance even in the presence of high magnetic fields. Hence, tremendous efforts have been devoted to realise long length superconducting tapes, which led to the 2nd generation high-temperature-superconductor (HTS) technology, the coated conductors. However, the production costs of REBCO coated conductors are still high, which may delay practical applications.

Chemical solution deposition (CSD) based on metal-organic deposition (MOD) using trifluoroacetate (TFA) precursors has been considered as very cost-effective process for REBCO coated conductors [1–3]. Although many parameters have to be optimised for obtaining excellent superconducting performance, the superconducting properties of REBCO thin films grown by CSD are comparable to those of films fabricated by pulsed laser deposition (PLD) [4, 5].

To date, nano-sized perovskite-type particles have been incorporated in REBCO superconducting matrices to improve the critical current density J_c in applied magnetic fields H even further. In fact, nanoparticle addition improves the J_c–H characteristics of REBCO grown by CSD dramatically without compromising T_c, which is in sharp contrast to PLD-grown REBCO films. For REBCO grown by PLD, the modulation of nano-strain due to the self-assembled perovskite nano-rods triggers the depletion of oxygen, resulting in lower T_c [6, 7]. To further improve the superconducting properties of CSD-grown REBCO, the underlying vortex pinning mechanism should be clarified.

Information on vortex pinning for a certain superconductor can be acquired by analysing i) the field dependence of J_c and ii) the angular dependence of J_c measured at various temperatures. Recently, the exponent n in the power-law relation $E \propto J^n$ (E electric field and J current density) has gained much attention for analysing the pinning, since unlike for low–T_c superconductors the exponent n provides insight into both the sample's homogeneity [8] and vortex creep [9, 10]. The importance of analysing n values for REBCO has been reported in several papers [11–15]. Here we report on the pinning mechanism of the CSD-grown $GdBa_2Cu_3O_{7-\delta}$+$BaHfO_3$ nanocomposite film by employing the methods mentioned above.

2. Experimental procedure

The $GdBa_2Cu_3O_{7-\delta}$ (GdBCO) thin film with 12 mol% nano-sized $BaHfO_3$ (BHO) particles was prepared by CSD. A concentration of 12 mol% of BaMO_3 (M = Zr, Hf), corresponding to $\sim$ 5 vol.%, has been considered optimum for CSD-grown REBCO (reference [14]), since tailoring of the BaMO_3 nanoparticles in the superconducting matrix is difficult unless, e.g. employing the well-designed processing route proposed in reference [16]. The preparation of the TFA solution used in this work is reported in reference [17]. In summary, the Gd, Ba and Cu acetates (purity> 99.99%, Alfa Aesar) and the Hf(IV) 2,4-pentanedionate (97+%, Alfa Aesar) are weighed out to give a stoichiometric 1:2:3 ratio and a 12 mol% BHO concentration in the final films with regard to Gd. Subsequently, they are dissolved in water and trifluoroacetic acid (TFAH, 99.5+%, Alfa Aesar) to convert the acetates into trifluoroacetates. After removing the water and other impurities by a rotary evaporator, the final dry powder is re-diluted in absolute methanol (99.9%) adjusting the concentration to 0.25 mol/l in Gd. This solution is deposited on $SrTiO_3$(001) substrates via spin coating (6000 rpm for 30 s) and then the samples are pyrolysed and grown using the optimised processes reported in [17] to finally obtain the GdBCO+12%BHO film studied in this work. As shown in [17], the GdBCO+12%BHO films grow epitaxially with almost no traces of undesired secondary phases. Additionally, no preferred orientation of BHO is confirmed.

The microstructure of the films were investigated using high-resolution and scanning transmission electron microscopy (HRTEM and STEM) via a C_s-corrected JEOL JEM 2200-FS instrument operated at 200 kV with bright-field (BF) and high-angle annular dark field (HAADF) detectors. Cross-sectional TEM lamellae were prepared via the focused-ion-beam technique in an FEI Nova 600 Nanolab Dual-Beam microscopy. The lamellae were extracted using an *in–situ* lift-out procedure with an Omniprobe extraction needle.

After microstructural characterisation, a small bridge for transport measurements was structured by photolithography and wet-chemical etching. The dimensions of the micro-bridge were 47 μm width, 1 mm length and 219 nm thickness, confirmed by atomic force microscopy (Bruker Dimension Edge AFM). To reduce the contact resistance, Au was deposited on the contact pads by PLD. The electrical resistivity was measured by a 4-probe method in a physical property measurement system (PPMS). The onset T_c was determined as the intersection between the linear fit to the normal state resistivity and the steepest slope of resistivity. The irreversibility line was determined by the resistivity criterion $\rho_c = E_c/J_{c,10}$, where E_c is the electric field criterion of 1 μVcm^{-1} for determining the critical current density J_c, and $J_{c,10} = 10\,Acm^{-2}$ is the corresponding criterion for the irreversibility field in J_c–H.

High-field electrical transport properties (d.c. fields up to $\mu_0 H = 19$ T with the 20 T cryogen-free superconducting magnet) were measured at IMR Tohoku university [18]. From E–J characteristics, the critical current density J_c was extracted using an electric field criterion E_c of 1 μVcm^{-1}. For measuring the angular dependence of J_c, the magnetic field H was applied in maximum Lorentz force configuration at different angles θ measured from the c-axis. Only at 77 K the angular dependence of J_c was measured in PPMS.

3. Results and discussion

BF-STEM images show that the film is dense with only minimal porosity and the BHO nano-particles (NPs) are homogeneously distributed in the matrix (figure 1(a)). It is also clear that a high density of intergrowths, called stacking faults (SFs) or $Gd_2Ba_4Cu_8O_{16}$ intergrowths and composed by double Cu-O planes, is observed in the upper region of the film. This tendency is quite common for CSD-grown REBCO films [19]. A more detailed view of the BHO NPs (figure 1(b)) reveals that their average size is $\sim$ 20 nm. They tend to crystallise randomly oriented with respect to the surrounding GdBCO matrix. These NPs are surrounded by SFs (figures 1(c) and (d)). It is also clear that BHO has faceted interfaces, which is similar to $BaZrO_3$ in YBCO grown by CSD [20]. Hence, highly incoherent interfaces between BHO and GdBCO are expected, which creates planar defects in CSD-grown films [21]. Those defects play an important role in the whole pinning scenario. The presence of the NPs generates a high-strain state distinguished by the black contrast in the cross-sectional BF-TEM image taken with a diffraction vector $\vec{g} = (100)$ (figure 1(e)). Also, the SFs and NPs break the twin-boundaries, presumably reducing their pinning effectivity in the c-axis direction.

The onset T_c was determined as 93.8 K (figure 2(a)), which is comparable to our standard GdBCO grown by CSD [17]. The film showed a sharp transition of $\Delta T_c = T_{c,onset} - T_{irr,0} \sim$ 0.8 K, indicating a high quality of our film. The irreversibility

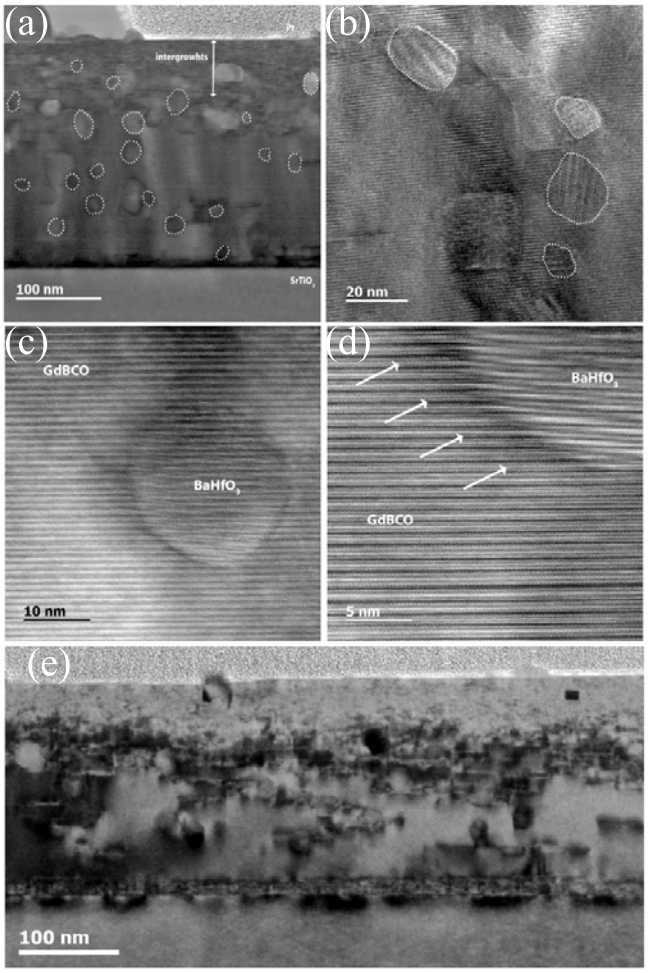

Figure 1. (a) Cross-sectional BF-STEM image of the GdBCO+12%BHO film grown on $SrTiO_3$. BHO nano-particles, which are surrounded by white dots for clarity, are finely dispersed in the superconducting matrix. High dense intergrowths is observed in the upper region of the film. (b) A more detailed view of the BHO NPs via HR-TEM reveals that the average size of BHO is $\sim$ 20 nm. They tend to crystallize randomly oriented with respect to the surrounding GdBCO matrix. (c) HAADF-STEM image of the interface between GdBCO and BHO. BHO has faceted interfaces, resulting in highly incoherent interface between BHO and GdBCO. (d) Several intergrowths presumably $Gd_2Ba_4Cu_8O_{16}$ indicated by white arrows are clearly seen in the high-resolution image of (c). (e) BF-TEM image taken with a diffraction vector $\vec{g} = (100)$. The black contrast indicates strain fields.

line exhibits a power relation $\sim (1 - T/T_{irr,0})^k$ with exponent $k = 1.29$ (figure 2(c)), which is close to the theoretically predicted value of 4/3 for glass-liquid transition in contrast to 3/2 for flux creep and 2 for melting [22].

Figure 3(a) summarises the J_c–H characteristics for GdBCO+BHO measured at various temperatures for $H \parallel c$. Self-field J_c and irreversibility field H_{irr} at 77 K were around 2.8 MAcm^{-2} and $\sim$ 10 T, which is consistent with the result obtained from the resistivity measurements (figure 2(c)). The maximum pinning force density F_p reached 7.8 GNm^{-3} at 2 T at 77 K (figure 3(b)). To acquire the information on vortex pinning profoundly, the normalised pinning force $f_p = F_p/F_{p,max}$ was plotted as a function of reduced field $h = H/H_{max}$ (figure 3(c)), where $F_{p,max}$ is the maximum F_p and H_{max} is the field at which F_p shows the maximum value. If f_p is plotted as a function of H/H_{max} instead of H/H_{irr} as the usual practice for HTS, one can analyse the pinning mechanism even though J_c could not be measured up to H_{irr}. Theoretically, f_p is described by the following formula,

$$f_p = \left(\frac{p}{q}\right)^q h^p \left(\frac{p+q}{p} - h\right)^q, \qquad (1)$$

which is analogous to the Dew-Hughes formula [23]. Substituting $(p, q) = (0.5, 2)$ into equation (1) leads to $f_p = \frac{25}{16} h^{0.5} \left(1 - \frac{h}{5}\right)^2$, which is identical to $\left(\frac{H}{H_{irr}}\right)^{0.5} \left(1 - \frac{H}{H_{irr}}\right)^2$ [24]. As can be seen in figure 3(c), equation (1) fits well the data acquired at 77, 65 and 50 K with $p = 0.50$, 0.46 and 0.47 under $q = 2$. All values were close to 0.5, indicating that the flux movement is dominated by shear of the flux line lattice at low fields and by plastic deformation at high fields proposed by Kramer [25]. The data at 30, 15 and 4.2 K are excluded, since $F_{p,max}$ could not be reached in fields up to 19 T. It was reported that the interface between $BaZrO_3$ particles and the superconducting matrix in CSD-grown YBCO creates strain fields. As the density of interfaces increases, a vast network of three-dimensional strained regions is constructed, resulting in quasi-isotropic pinning behaviour [20]. This mechanism may also prevail for GdBCO+BHO.

By using the exponent values p and q, H_{irr} is calculated to be 10, 22 and 37 T at 77, 65 and 50 K, respectively. These values fall onto the irreversibility line shown in figure 2(c).

Another direction for analysing the pinning mechanisms is to look at the E–J characteristics for determining J_c. For REBCO, the E–J curves exhibit a power-law relation $E \propto J^n$ if the sample is homogeneous and free of grain boundaries. Since the exponent n is proportional to the pinning potential, J_c usually scales positively with n, and empirically a relation $(n–1) \propto J_c^{\alpha}$ was found [27]. In fact, this can be seen in figure 4(a). For $H \parallel c$ the relation $(n\text{-}1) \propto J_c^{0.45}$ is almost followed irrespective of measurement temperature. The data for the high-J_c regime (*i.e.* below 65 K and low fields) deviate from the master curve towards lower n values due probably to a second pinning mechanism setting in. Another plausible reason is that the scaling is valid for fields not too far away from H_{irr} only, since it is related to the critical exponents of the glass-liquid scaling. Somewhat higher n values at 4 K compared to the scaling function might indicate slight Joule heating of the sample during measurement. For $H \parallel ab$ the data at 77 K falls onto the master curve $(n\text{-}1) \propto J_c^{0.45}$ (figure 4(b)), whilst all data at 65 and 50 K deviate from the master curve.

For further insight into the pinning mechanism, the angular dependence of J_c ($J_c(\theta)$) and the corresponding $n(\theta)$ were measured at 77, 65, 50 and 30 K in various magnetic fields as summarised in figure 5. Thanks to the BHO addition, the anisotropy of J_c (*i.e.* the ratio of J_c for $H \parallel ab$ and c) is rather small at low magnetic fields: e.g. J_c^{ab}/J_c^{c} is around 1.4 at 77 and 65 K and 3 T. With increasing magnetic field towards H_{irr}, a J_c

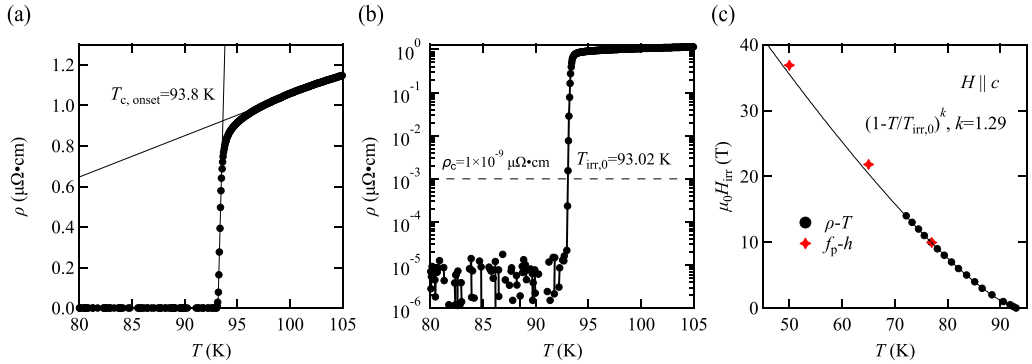

Figure 2. (a) Resistivity curve for GdBCO+BHO measured in the absence of magnetic field. (b) Semi-logarithmic plot of (a). Dashed line indicates the resistivity criterion for determining the irreversibility temperature T_{irr}. In self-field the T_{irr} was 93.02 K. (c) The irreversibility line for $H \| c$ was determined by the field dependence of resistivity measurements. The irreversibility fields evaluated from the pinning force analyses well follows the irreversibility line.

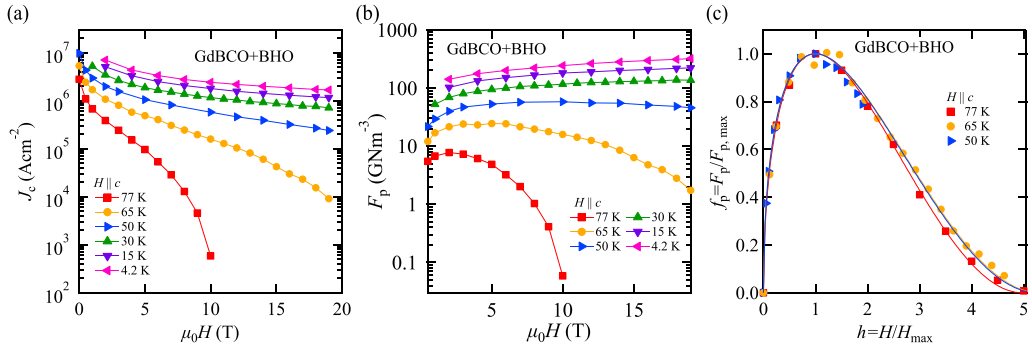

Figure 3. Field dependence of (a) J_c and (b) F_p for GdBCO+BHO measured at various temperatures. The applied field was parallel to the c-axis. Below 30 K and low field regime J_c could not be measured due to sample heating. (c) The normalised pinning force density $f_p = F_p/F_{p,max}$ versus reduced field $h = H/H_{max}$. Fits of equation (1) to each f_p with fixed $q = 2$ is superimposed.

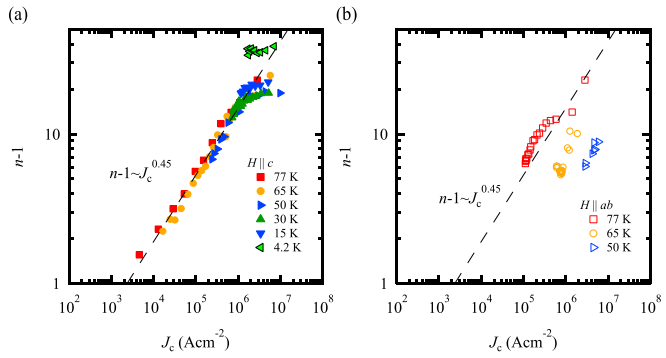

Figure 4. Relationship between n and J_c for (a) $H \| c$ and (b) $H \| ab$.

peak for $H \| c$ is progressively apparent, which is explained by the competition between random pinning and c-axis correlated growth defects, such as dislocations and anti-phase boundaries [33]. However, this peak is rather smeared at 50 K due to the small relative magnetic fields H/H_{irr}.

The angular dependence of n behaves similarly to that of J_c for the angle regime -30° < θ < 70°. However, when the field direction is close to the ab-plane, the above scaling is violated. For $H \| ab$, the exponent n shows a dip at 77 K in the low field regime, although J_c shows a maximum (figure 5(a)). But this dip disappears when the magnetic field is increased. Further increasing of H leads to the upturn of n. Jha *et al* recently showed very similar angular dependencies not for the n value but rather for J_c itself for PLD-grown Y_2BaCuO_5-YBCO nanocomposite films [28]. They explained this behaviour by a competition between different sets of pinning centres, namely the isotropic Y_2BaCuO_5 nanoparticles and the stacking faults, regarding their pinning potential, U. The same arguments may hold in our case: In the framework of Zeldov's model of a logarithmic current density dependence of the pinning potential [29], the n value is directly related to U [30]. The angular dependencies of U are shown in [28]: Whereas isotropic defects show an angular dependence related (but not necessarily equal) to the electronic mass anisotropy, the correlated defects show a peak for fields parallel to their direction, related to the accommodation of vortices in these defects for angles between the applied field and defect direction smaller than the so-called accommodation angle θ_{acc} ($\tan\theta_{acc} = \sqrt{2u_p/\epsilon_l}$, u_p the pinning energy per unit length of the defect), which is related to the line tension (ε_l) of the vortices. This is exactly what is observed for high temperatures (77 K). At low fields, the pinning potential of the large random pinning centres ($BaZrO_3$ nanoparticles) surpasses the pinning potential of the stacking faults leading to broad maxima of

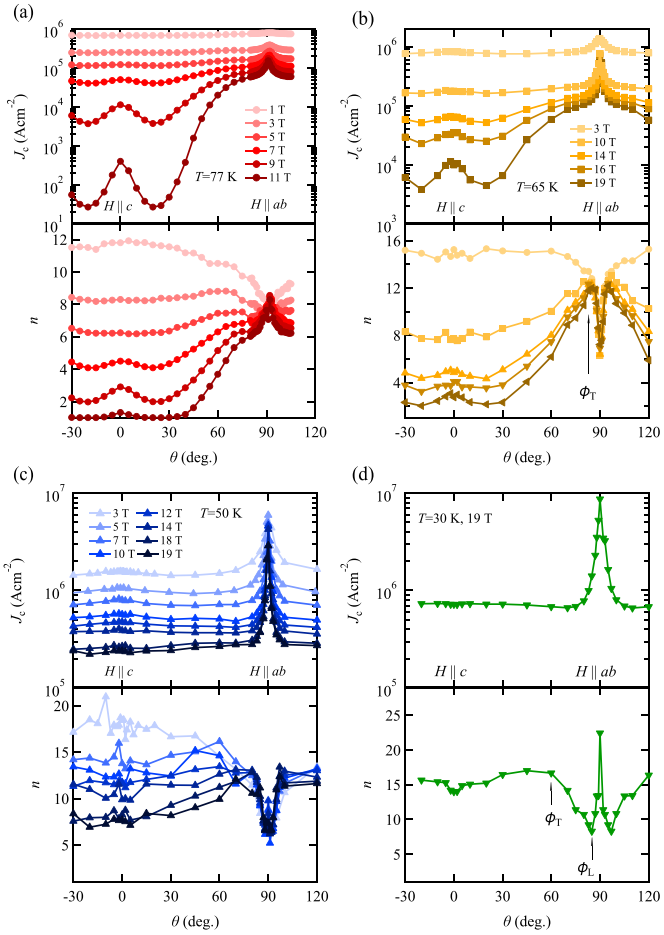

Figure 5. Angular dependence of J_c and the corresponding n value measured at (a) 77, (b) 65, (c) 50 and (d) 30 K in the presence of various magnetic fields.

n near $H \| c$ (with shoulders at intermediate angles). At high fields, the pinning potential of the correlated defects (both *ab*-directional stacking faults and *c*-directional growth defects such anti-phase boundaries and dislocations) is higher leading to peaks in n value and J_c. The dip in n value can be described and explained by scaling approaches taken into account the size of random pinning centres [31] or in statistical, maximum-entropy considerations [32]. The reason for the fact that these dependencies are observed for the n value in our case but for J_c in reference [28] is not totally clear but may be related to the differences in microstructure, which is in reality much more complex.

At temperatures of 65 K and below, the dip of n near the *ab*-direction is formed at all magnetic fields investigated and the deep minimum is almost constant irrespective of applied magnetic fields. Compared to the data at 77 K, this minimum has a different reason. The dimensional crossover between the out-of-plane superconducting coherence length $\xi_c(T)$ and the CuO_2 interlayer distance d occurs around this temperature, as also observed for TFA-MOD grown (Y,Gd)BCO films with $BaZrO_3$ [13] and pure YBCO grown by chemical vapour deposition [33]. The dip formation is due to the enhanced thermal movement of kinked vortices [34], since n is fundamentally related to the flux creep rate $S = 1/(n-1)$ [35]. Parts of the vortices are trapped by the regions of reduced order parameter and connected by vortex kinks, thus forming a stair case structure. In contrast to the data at 77 K, $n(\theta)$ is independent of applied field within the dip (*i.e.* trapping) region since the creep rate, and hence the n value, only depends on the number of kinks per unit length of flux line.

The onset angle β of the decrease of n is related to the vortex trapping angle (ϕ_T), which is defined as $\phi_T = 90^\circ - \beta$. The respective ϕ_T at 65, 50 and 30 K at the maximum field are 5°, 10° and 20°. According to figures 4(a), 5(a) and (b) the intrinsic pinning, originating from the modulation of the superconducting order parameter, starts to be active slightly above 65 K. The out-of-plane coherence length at zero kelvin, $\xi_c(0)$, is estimated to be ~ 0.22 nm by $\xi_c(0) = \frac{d}{2}\sqrt{1 - T_{cr}/T_c}$, where $d = \frac{2}{3}c = 0.78$ nm (c is the c-axis length determined by x-ray diffraction) is the interlayer distance and T_{cr} is the the dimensional crossover temperature (*i.e.* $T_{cr} \sim$65 K). The estimated value is close to the one for YBCO [36]. At 50 K, tiny peaks in the valley appear, and the peak grows prominently at 30 K. This phenomenon is related to the vortex lock-in, where all vortices are parallel to the *ab*-planes and locked between the CuO planes even though the applied field may be inclined slightly away from the planes. In this case, very strong pinning is created, the creep rate is decreased strongly due to the absence of kinks, and hence n is increased. The respective vortex lock-in angle ϕ_L at 50 and 30 K under $\mu_0 H = 19$ T are around 2° and 5°. It was reported that both ϕ_T and ϕ_L in YBCO are affected by nano-inclusions [37]. Both these characteristic angles for $BaZrO_3$-containing YBCO are larger than those for pure YBCO. It could be interesting to investigate if this tendency is also valid for GdBCO as assumed. These studies would be our future direction.

4. Conclusion

The pinning properties of a $GdBa_2Cu_3O_{7-\delta}$ thin film with 12 mol% of nano-sized $BaHfO_3$ (BHO) particles have been investigated by measuring field and angular dependences of electric transport J_c at various temperatures in fields up to 19 T. For $H \| ab$, J_c is dominated by intrinsic pinning below 77 K. The vortex trapping angle and lock-in angle are increased with decreasing temperature. The n-value analysis is a powerful tool for investigating the pinning mechanism especially for $H \| ab$.

Acknowledgment

This work was supported by Japan-Germany Research Cooperative Program between JSPS and DAAD, Grant number JPJSBP120203506. A part of this work was performed at High Field Laboratory for Superconducting Materials, Institute for Materials Research, Tohoku University (Project No. 19H0507).

References

[1] Knoth K, Engel S, Apetrii C, Falter M, Schlobach B, Hühne R, Oswald S, Schultz L and Holzapfel B 2006 *Current Opinion in Solid State and Materials Science* **10** 205

[2] Albiss B A and Obaidat I M 2010 *J. Mater. Chem.* **20** 1836

[3] Bäcker M, Baumann A, Brunkahl O, Erbe M, Schneller T *et al* 2020 Chemical Solution Deposition (CSD) *Encyclopedia of Applied Physics* (Hoboken: Wiley) VVerlag Gmbh CH and Kgaa Co (Ed.)

[4] Erbe M *et al* 2015 *Supercond. Sci. Technol.* **28** 114002

[5] Rijckaert H *et al* 2020 *Coatings* **10** 17

[6] Cantoni C, Gao Y, Wee S H, Specht E D, Gazquez J, Meng J, Pennycook S J and Goyal A 2011 *ACS Nano* **5** 4783

[7] Horide T, Kametani F, Yoshioka S, Kitamura T and Matsumoto K 2017 *ACS Nano* **11** 1780

[8] Warnes W H and Larbalestier D C 1986 *Appl. Phys. Lett.* **48** 1403

[9] Yeshurun Y, Malozemoff A P and Shaulov A 1996 *Rev. Mod. Phys* **68** 911

[10] Sun J Z, Eom C B, Lairson B, Bravman J C and Geballe T H 1991 *Phys. Rev.* B **43** 3002

[11] Civale L, Maiorov B, MacManus-Driscoll J L, Wang H, Holesinger T G, Foltyn S R, Serquis A and Arendt P N 2005 *IEEE. Trans. Appl. Supercond.* **15** 2808

[12] Tarantsev E F, Strickland N M, Hoefakker P, Xia J A and Long N J 2008 *Current Applied Physics* **8** 388

[13] Awaji S, Namba M, Watanabe K, Miura M, Yoshizumi M, Izumi T and Shiohara Y 2010 *Supercond. Sci. Technol.* **23** 014006

[14] Palau A, Bartolomé E, Llordés A, Puig T and Obradors X 2011 *Supercond. Sci. Technol.* **24** 125010

[15] Chudy M, Zhong Z, Eisterer M and Coombs T 2015 *Supercond. Sci. Technol.* **28** 035008

[16] Miura M *et al* 2017 *NPG Asia Mater.* **9** e447

[17] Cayado P, Erbe M, Kauffmann-Weiss S, Bühler C, Jung A, Hänisch J and Holzapfel B 2017 *Supercond. Sci. Technol.* **30** 094007

[18] Awaji S *et al* 2014 *AIP Conf. Proc.* **1573** 732

[19] Li Z *et al* 2019 *Sci. Rep.* **9** 5828

[20] Llordés A *et al* 2012 *Nat. Mater.* **11** 329–36

[21] Molina-Luna L, Duerrschnabel M, Turner S, Erbe M, Martinnez G T, Van Aert S, Holzapfel B and Van Tendeloo G 2015 *Supercond. Sci. Technol.* **28** 115009

[22] Schilling A, Ott H R and Wolf T 1992 *Phys. Rev.* B **46** 14253

[23] Dew-Hughes D 1974 *Philos. Mag.* **30** 293

[24] Higuchi T, Yoo S I and Murakami M 1999 *Phys. Rev.* B **59** 1514

[25] Kramer E J 1973 *J. Appl. Phys.* **44** 1360

[26] Awaji S, Namba M, Watanabe K, Ito S, Aoyagi E, Kai H, Mukaida M and Okayasu S 2011 *IEEE. Trans. Appl. Supercond.* **21** 3192

[27] Opherden L *et al* 2016 *Sci. Rep.* **6** 21188

[28] Jha A K, Matsumoto K, Horide T, Saini S, Mele P, Ichinose A, Yoshida Y and Awaji S 2017 *J. Appl. Phys.* **122** 093905

[29] Zeldov E, Amer N M, Koren G, Gupta A, McElfresh M W and Gambino R J 1990 *Appl. Phys. Lett.* **56** 680

[30] Guarino A, Leo A, Grimaldi G, Martucciello N, Dean C, Kunchur M N, Pace S and Nigro A 2014 *Supercond. Sci. Technol.* **27** 124011

[31] Mishev V, Zehetmayer M, Fischer D X, Nakajima M, Eisaki H and Eisterer M 2015 *Supercond. Sci. Technol.* **28** 102001

[32] Long N J 2013 *J. Supercond. Nov. Magn.* **26** 763

[33] Awaji S, Ishihara R, Watanabe K, Shikimachi K, Hirano N and Nagaya S 2011 *Appl. Phys. Express* **4** 013101

[34] Maiorov B, Baily S B, Zhou H, Ugurlu O, Kennison J A, Dowden P C, Holesinger T G, Foltyn S R and Civale L 2009 *Nat. Mater.* **8** 398

[35] Yamasaki H and Mawatari Y 1999 *IEEE. Trans. Appl. Supercond.* **9** 2651

[36] Camerlingo C and Jung G 2005 *Supercond. Sci. Technol.* **18** 1106

[37] Weigand M, Zhou H, Foltyn S R, Civale L and Maiorov B 2012 Temperature dependence of pinning near $H \parallel ab$ in YBCO thin films *Applied Superconductivity Conference* 3ME-03 (http://www.ascinc.org/asc2012/wp-content/uploads/file/ASC2012_Digital_Program_Book_Updated.pdf)